Investigation of a $p-i-n$ photodetector with an absorbing medium based on InGaAs/GaAs quantum well-dots

© N.V. Kryzhanovskaya[1], S.A. Blokhin[2,1], I.S. Makhov[1], E.I. Moiseev[1], A.M. Nadtochiy[1], N.A. Fominykh[1], S.A. Mintairov[2], N.A. Kaluyzhnyy[2], Yu.A. Guseva[2], M.M. Kulagina[2], F.I. Zubov[3,1], E.S. Kolodeznyi[4], M.V. Maximov[3,1], A.E. Zhukov[1]

[1] HSE University,
190008 St. Petersburg, Russia
[2] Ioffe Institute,
194021 St. Petersburg, Russia
[3] Alferov University,
Saint Petersburg National Research Academic University of the Russian Academy of Sciences,
194021 St. Petersburg, Russia
[4] ITMO University,
197101 St. Petersburg, Russia

E-mail: nataliakryzh@gmail.com

Received March 21, 2023
Revised March 23, 2023
Accepted April 20, 2023

The static and dynamic characteristics of waveguide photodetectors with an absorbing region based on InGaAs/GaAs quantum well-dots were studied at room temperature. The absorption band of InGaAs/GaAs quantum well-dots is in the spectral range from 900 to 1100 nm. The waveguide photodetectors have a width of 50 μm and a length of the absorbing region from 92 μm to 400 μm. A low dark current density (1.1 and 22 μA/cm^2 at -1 and -20 V) and cut off frequency of 5.6 GHz, limited by the time constant of a parasitic equivalent electric *RC*-circuit, were obtained.

Keywords:waveguide photodetector, modulation frequency, quantum well-dots, integrated photonics.

DOI: 10.21883/SC.2023.03.56236.4727

1. Introduction

Waveguide photodetectors (WGPD) are promising components of optical integrated circuits that require light detection in the integrated circuit plane (i.e., light coupling into an end facet). The design of a waveguide photodetector based on a waveguide $p-i-n$-structure [1], where the photon flux and the motion of photogenerated carriers are orthogonal, is widely used to provide high sensitivity and speed. In such waveguide photodetectors, the path of radiation absorption correspond to the length of the strip and, therefore, can be significantly increased compared to planar photodetectors, whereas the path of passage of the photogenerated charge carrier corresponds to the thickness of the semiconductor layer of the waveguide By now, in waveguide $p-i-n$ photodetectors based on germanium and $A^{III}B^{V}$ materials, an optical bandwidth of > 50 GHz [2–4] has been demonstrated. The disadvantage of a waveguide photodetector is its low resistance to lateral and vertical displacement of the input signal incident on the receiving surface of the photodetector. In integrated photonics devices, mutual alignment of a light source based on $A^{III}B^{V}$ materials and a waveguide photodetector on the same substrate should be implemented with monolithic integration [5] or when they are combined as a result of hybrid integration processes [6]. Another problem of photodetectors is to minimize the parasitic time constant of the equivalent electrical *RC*circuit in order to obtain high speed photodetectors, which is usually realized by reducing the active area, pad capacitance and series resistance. On the other hand, the low output power of miniature radiation sources requires a large absorption path in the photodetector [7], i.e. active area, which leads to an increase in the time constant.

In this paper, an array of InGaAs/GaAs quantum well-dots (QWDs) is used to implement efficient light absorption in a photodetector. Due to the high density of the InGaAs/GaAs QWD array, a high value of the saturated material gain of one QWD layer $1.5 \cdot 10^4$ cm^{-1} [8] is realized in them. Saturated modal absorption during lateral light propagation was estimated to be 69 cm^{-1} per one QWD layer [9]. In the paper [10] it was shown that waveguide photodetectors based on InGaAs/GaAs QWDs can effectively detect radiation from disk microlasers with lateral light extraction operating in a continuous-wave mode. In the present paper, photocurrent spectra measured in a wide spectral range, as well as the high-frequency response of photodetectors implemented in the form of a strip with a width of 50 μm and different lengths using an external high-speed vertical-cavity surface-emitting laser (VCSEL) with a radiation wavelength of 905 nm are investigated.

2. Experiment description

The epitaxial heterostructure was grown by metalorganic vapor-phase epitaxy at reduced pressure and 500–700°C

temperatures using hydrogen as a carrier gas. The structure consists of *n*- and *p*-doped $Al_{0.39}Ga_{0.61}As$ *p*- and *n*-layers and an undoped GaAs waveguide layer 0.78 μm thick. The absorbing area is placed in a GaAs waveguide and contains 6 InGaAs/GaAs QWD layers. Each QWD layer was formed by the deposition 8 $In_{0.4}Ga_{0.6}As$ monolayers and separated from the adjacent layer by a 40 nm thick GaAs spacer (Fig. 1).

Misoriented GaAs [11] substrates were used to form pronounced thickness and composition heterogeneities in InGaAs/GaAs QWD layers. Strip structures 50 μm wide were fabricated by photolithography and dry etching (STE ICPe68). The mesa height was $\sim 5.5\,\mu$m. To create an Ohmic contact to the p^+-GaAs contact layer, a composite AgMn/Ni/Au contact with a total thickness of $0.1-0.15\,\mu$m was formed on the strip surface. The AuGe/Ni/Au metallization was used to form a solid Ohmic contact with the *n*-GaAs substrate. The light-absorbing facets of the photodiode structures were formed by splitting photodetector crystals without applying additional antireflection coatings. A series of photodetector crystals of various lengths 92, 217, 322 and 400 μm was formed (Fig. 2, *a*).

Studies of the photocurrent of photodetectors with QWD were performed by illuminating the facet surface of the photodetector with radiation with a selected wavelength in the spectral range 800–1200 nm. For this purpose, we used the radiation of a halogen lamp passed through a Spectral Products D480 monochromator. A Keithley 2401 source-meter unit was used to measure the photocurrent. To analyze the frequency response, each photodetector was mounted by soldering with the *n*-contact down on the G (ground) area of the ceramic board pad with contact pad metallization in the high-frequency GSG topology (Fig. 2, *b*). Meanwhile, *p*-photodetector pin was electrically connected with a gold wire to the S (signal) pad of the board.

The PNA N5234B network analyzer was used to measure electrical reflection (parameters S11, S22) and response on small-signal modulation of incident light (parameter S21). The frequency response of photodetectors (PD) was measured at a specific wavelength. An In(Al)GaAs/GaAs vertical-cavity surface-emitting laser with a wavelength of 905 nm was used as a source of modulated radiation. It should be noted that the recorded response of the photodetector was associated exclusively with light absorption in the InGaAs/GaAs QWDs, while the GaAs matrix remained transparent for the given laser wavelength. The radiation from the VCSEL operating in the mode of high-frequency modulation of the pump current was collected using a lensed optical fiber and transmitted through a multimode optical fiber. From the other end, this fiber was connected to a fiber optic probe with a microlens, which focused the VCSEL radiation on the end facet of the photodetector. The resulting amplitude-frequency characteristic (AFC) of the studied photodetector was then corrected taking into account the AFC of the VCSEL, determined using a high-speed IR photodetector Newport 1414-50.

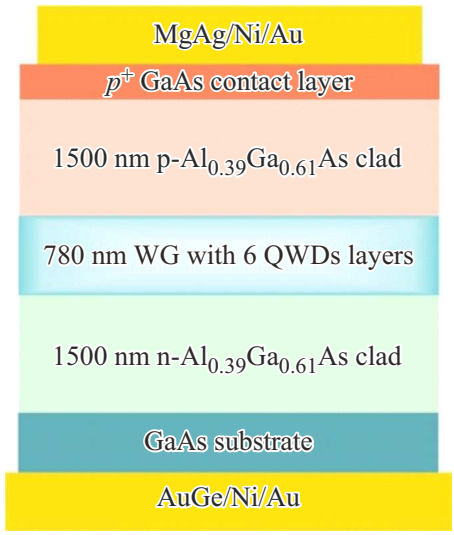

Figure 1. Schematic representation of the layer sequence of the epitaxial heterostructure of a photodetector with InGaAs/GaAs quantum well-dots.

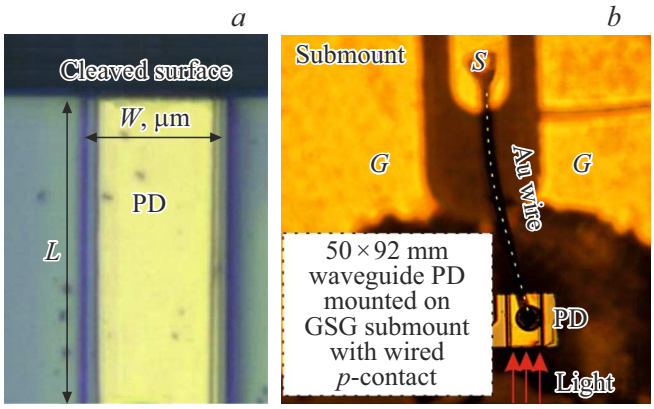

Figure 2. Images obtained with an optical microscope, of the PD $50 \times 182\,\mu$m, top view (*a*) and PD $50 \times 92\,\mu$m, placed on a GSG board (it b).

3. Results and discussion

First, the current-voltage characteristics of a rectangular photodetector $50 \times 92\,\mu$m without illumination were studied. The measured dark current of photodiodes at reverse bias -1 V was 0.05 nA (Fig. 3), which corresponds to a dark current density of $1.1\,\mu A/cm^2$. We previously reported a dark current density of $20\,\mu A/cm^2$ for a QWD-based photodetector at a reverse voltage of 1 V [12]. For comparison, dark current density values of 80 [7], 40 [13], $0.4\,\mu A/cm^2$ [14] were reported for the same bias value. A low dark current (1 nA, $22\,\mu A/cm^2$) is retained with an increase in the reverse bias, at least up to -20 V, which indicates a high structural perfection of the epitaxial layers of the photodetector heterostructure and a low level of surface leakage.

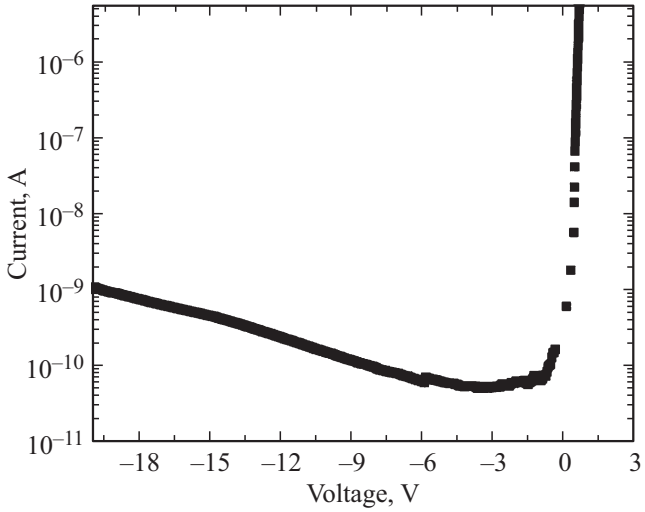

Figure 3. Current-voltage characteristic of the photodetector $50 \times 92\,\mu$m.

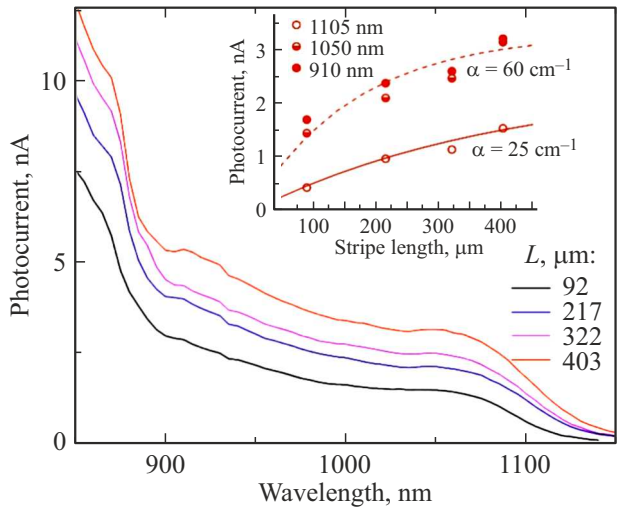

Figure 4. Dependence of the photocurrent on the wavelength of the light incident on the 50-μm facet of the photodetector for devices of different lengths. The insert shows the dependence of the photocurrent on the stripe length (L) for various recorded wavelengths (910, 1050, and 1105 nm).

The PD spectral response band corresponding to absorption in the InGaAs/GaAs QWDs covers the area from 900 to 1130 nm (Fig. 4). At the incident radiation wavelength < 890 nm, a sharp increase in the photocurrent is observed, which is associated with absorption in the GaAs waveguide. An increase in the length of the photodetector L (the length of the absorbing region) from 92 to $\sim 200\,\mu$m leads to a noticeable increase in the detector photocurrent (see the inset to Fig. 4). With a further increase in the length of the photodiode to $400\,\mu$m, the increase in photocurrent becomes smaller, which indicates absorption saturation, since the length of the photoabsorbing media becomes comparable to the characteristic light penetration length ($\sim 1/\alpha$). Fitting the data using the $1 - \exp(-\alpha L)$ function allowed to estimate the value of the modal absorption $\alpha \sim 25\,\text{cm}^{-1}$ for long-wavelength (wavelength 1105 nm) and $\sim 60\,\text{cm}^{-1}$ (wavelength 910 and 1050 nm) for the main spectral absorption area of quantum well-dots.

S21 curves were obtained for all photodetectors, characterizing the frequency response of photodetectors, in the range of reverse bias voltages from 0 to -20 V. Figure 5 shows S21 curves for a photodetector with a length of $92\,\mu$m. The bandwidth of $f_{3\text{dB}}$ was determined at the level of signal intensity of — 3 dB. As can be seen, an increase of reverse bias applied to the photodetector from 0 to -10 V leads to an increase in its bandwidth from 0.8 to 5.1 GHz.

The dependences of the $f_{3\text{dB}}$ bandwidth on the bias voltage for all lengths of the studied photodetectors are shown in Fig. 6. The dependences obtained for $f_{3\text{dB}}$ in a

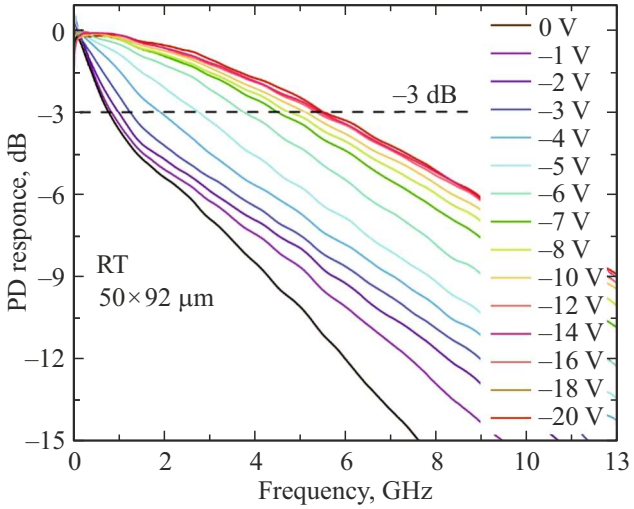

Figure 5. Dependences of the high-frequency response of PD $50 \times 92\,\mu$m, measured at various reverse bias voltages.

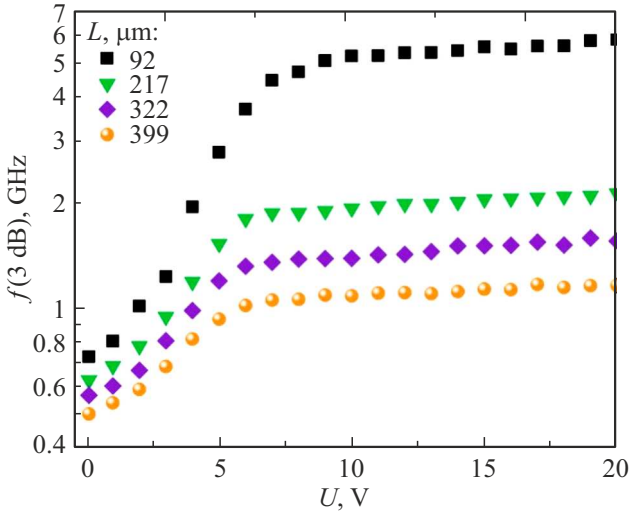

Figure 6. Frequency dependences of $f_{3\text{dB}}$ on the bias voltage for all lengths of the studied photodetectors.

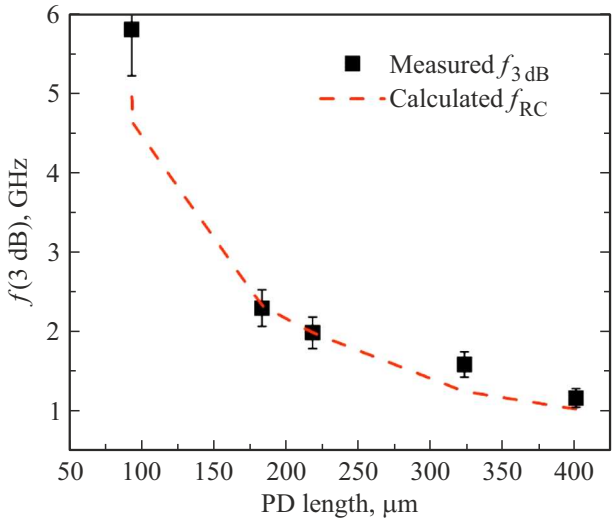

Figure 7. Experimental values of f_{3dB} (squares) and calculated cut-off frequency f_{RC} (dotted line) depending on the length of the studied photodetectors.

waveguide photodetector are determined by two processes. In the area of low reverse bias voltages, the frequency is limited by the transition time of photogenerated charge carriers from the absorbing region to the contacts (transition time, t). In this case, the limiting values of the frequency f_t associated with carrier transport ($f_t \sim 1/t$) are presumably determined by the low drift velocity of holes in GaAs, which depends on the electric field strength in the i area. Increasing the reverse bias allows to increase the speed of the photodetector to a certain limiting frequency value, after which the observed dependences saturate at a bias voltage of more than $-7--10$ V. A further increase in voltage causes only a slight increase in the cutoff frequency (up to 5.8 GHz at 20 V for a PD with a length of 92 μm). The observed saturation is related to the *RC*-recharge time of the RC-circuit, which is independent on the bias voltage:

$$f_{RC} \sim \frac{1}{2\pi R(C_j + C_p)},$$

where R — load resistance (usually 50 Ohm), C_j — photodetector capacitance, C_p — contact pad capacitance. The fact that the limiting frequency f_{3dB} decreases with increasing length of the photodetector suggests that the bandwidth of the photodetector is limited mainly by its capacitance, which increases with the area of the photodetector.

To estimate the limiting cut-off frequency of f_{RC}, we determined the parameters of the photodetector equivalent scheme by fitting the real and imaginary parts of the S22 parameter using the Qucs electrical circuit simulator. The capacitance of the photodetector decreases proportionally to its area from 2840 fF to 670 fF, while the specific capacitance of the photodetector reaches 0.14 fF/μm^2. The series resistance Rs of the photodetectors was $Rs \sim 4-5$ Ohm. The capacitance of the contact pads of the ceramic board does not exceed 60 fF, and the inductance of the gold wire connecting the p-photodetector contact with the S-pad lies in the range of 450−500 pG. Fig. 7 shows the cut-off frequencies f_{RC} calculated from the reconstructed equivalent schemes of the studied photodetectors. It can be seen that the obtained maximum values of the f_{3dB} frequency bandwidth for all photodetectors are determined by the time constant of the parasitic equivalent electrical *RC*-circuit.

4. Conclusion

In the paper, static and dynamic area were investigated at room temperature of waveguide photodetectors with 6 layers of InGaAs/GaAs quantum well dots used as the absorbing area. The spectral absorption band of InGaAs/GaAs quantum well-dots is in the range from 900 to 1100 nm. A low value of the dark-current density of 1.1 μA/cm^2 and a limiting speed of 5.6 GHz, limited by the time constant of a parasitic equivalent electrical *RC*-circuit for a photodetector with a size of $50 \times 92\,\mu$m, are obtained. The analysis of the mechanisms that restrict the limiting speed of devices showed the need to reduce the transition time in the i area for holes and reduce the area of devices aiming to decrease the time constant of a parasitic equivalent electrical *RC*-circuit. In the current implementation, such photodetectors can be successfully used for integration with planar emitting microlasers to create all-optical high-speed data transmission channels and optical sensors.

Acknowledgments

The work was carried out on the equipment of the large-scale research facilities „Complex optoelectronic stand of the National Research University Higher School of Economics — Saint-Petersburg“.

Funding

The studies were carried out as part of the Fundamental Research Program of the National Research University Higher School of Economics. The work of E.S. Kolodezny was financially supported by the program „Priority 2030“ in terms of studying the photocurrent of detectors.

Conflict of interest

The authors declare that they have no conflict of interest.

References

[1] J.E. Bowers, C.A. Burrus. Electron. Lett., **22**, 905 (1986).
[2] H. Wang, J. Zhang, G. Zhang, Y. Chen, Y.-C. Huang, X. Gong. Optics Lett., **46**, 2099 (2021).

[3] L. Vivien, A. Polzer, D. Marris-Morini, J. Osmond, J.M. Hartmann, P. Crozat, E. Cassan, C. Kopp, H. Zimmermann, J.M. Fédéli. Opt. Express, **20**, 1096 (2012).
[4] K. Kato, A. Kozen, Y. Muramoto, Y. Itaya, T. Nagatsuma, M. Yaita. IEEE Phot. Techn. Lett., **6**, 719 (1994).
[5] Y. Wan, Z. Zhang, R. Chao, J. Norman, D. Jung, C. Shang, Q. Li, M. Kennedy, D. Liang, C. Zhang, J. Shi, A.C. Gossard, K.M. Lau, J.E. Bowers. Opt. Express, **25**, 27715 (2017).
[6] A. Beling, A.S. Cross, M. Piels, J. Peters, Q. Zhou, J.E. Bowers, J.C. Campbell. Opt. Express, **21**, 25901 (2013).
[7] Y. Wan, C. Shang, J. Huang, Z. Xie, A. Jain, J. Norman, B. Chen, A.C. Gossard, J.E. Bowers. ACS Nano, **14**, 3519 (2020).
[8] N.Yu. Gordeev, M.V. Maximov, A.S. Payusov, A.A. Serin, Yu.M. Shernyakov, S.A. Mintairov, N.A. Kalyuzhnyy, A.M. Nadtochiy, A.E. Zhukov. Semicond. Sci. Techn., **36**, 015008 (2021).
[9] A.M. Nadtochiy, N.Yu. Gordeev, A.A. Kharchenko, S.A. Mintairov, N.A. Kalyuzhnyy, Y.S. Berdnikov, Y.M. Shernyakov, M.V. Maximov, A.E. Zhukov. J. Lightwave Technol., **39**, 7479, (2021).
[10] N.V. Kryzhanovskaya, F.I. Zubov, E.I. Moiseev, A.S. Dragunova, K.A. Ivanov, M.V. Maximov, N.A. Kaluzhnyy, S.A. Mintairov, S.V. Mikushev, M.M. Kulagina, J.A. Guseva, A.I. Likhachev, A.E. Zhukov. Las. Phys. Lett., **19**, 016201 (2022).
[11] A.M. Nadtochiy, M.V. Maximov, S.A. Mintairov, N.A. Kalyuzhnyy, V.N. Nevedomskiy, S.S. Rouvimov, A.E. Zhukov. Phys. Status Solidi B, **255**, 1800123 (2018).
[12] A. Zhukov, S. Blokhin, N. Maleev, N. Kryzhanovskaya, E. Moiseev, A. Nadtochiy, S. Mintairov, N. Kalyuzhnyy, F. Zubov, M. Maximov. Opt. Express, **29** (25), 40677 (2021).
[13] D. Inoue, Y. Wan, D. Jung, J. Norman, C. Shang, N. Nishiyama, S. Arai, A.C. Gossard, J.E. Bowers. Appl. Phys. Lett., **113**, 093506 (2018).
[14] J. Huang, Y. Wan, D. Jung, J. Norman, C. Shang, Q. Li, K.M. Lau, A.C. Gossard, J.E. Bowers, B. Chen. ACS Photonics, **6**, 1100 (2019).

Translated by E.Potapova